Proceedings of the ASME 2010 3rd Joint US-European Fluids Engineering Summer Meeting and 8th International Conference on Nanochannels, Microchannels, and Minichannels
FEDSM-ICNMM2010
August 1-5, 2010, Montreal, Canada

FEDSM-ICNMM2010-30111

THE OPTIMIZATION OF PARALLEL CHANNEL PATTERNS DESIGN ON MICRO METHANOL STEAM REFORMER

Jiin-Yuh Jang
Department of Department of Mechanical Engineering
National Cheng-Kung University
Tainan, Taiwan

Yu-Xian Huang
Department of Department of Mechanical Engineering
National Cheng-Kung University
Tainan, Taiwan

Chin-Hsiang Cheng
Department of Aeronautics and Astronautics
National Cheng-Kung University
Tainan, Taiwan

ABSTRACT

This study was aimed at the performance of micro methanol steam reformer for channel widths optimization by simplified conjugate gradient method (SCGM) with minimum objective function of velocity standard deviation. A three-dimensional numerical model and optimal algorithm named simplified conjugate gradient method (SCGM) were built for predicting the dominating factors in channel widths. In the optimization searching process, the simulation model only includes the continuity and the momentum equations for decreasing the computational time. When the optimum channel width of different inlet flow rate and its distributions are obtained by SCGM with minimum objective function, the species and energy equations are applied to evaluate the performance of steam reformer. Distributions of velocity were predicted, and the methanol conversion ratio was also evaluated. In addition, the mole fraction of CO contained in the reformed gas, which is essential to prevent the catalyst layers of fuel cells from poisoning, is also investigated. Furthermore, the present simulation model was also compared with existing experiment data, and the close agreement was found. Results show that the methanol conversion ratio can be improved from 54.2% to 62.6% for the particular case at 0.6 cc/min flow rate if the channel widths are optimized. On the other hand, the mole fraction of carbon monoxide is increased from 2.85 % (original) to 5.21 % (optimal) at $\dot{Q}$ =0.6 cc min^{-1}.

Keywords: Micro reformer; Steam reforming; Methanol conversion ratio; Hydrogen production rate.

INTRODUCTION

There have been many significant studies arose for mini power generation unit in recent years. Small-scale polymer electrolyte membrane fuel cells (PEMFC) are regarded as potential power sources for portable electronic devices. When the small-scale fuel cells are applied, it is essential to develop a hydrogen supplier of equal size such that the entire volume of the power source unit will not be remarkably increased. Hydrogen gas may be released or produced from metal hydrides, chemical hydrides, and hydrocarbon fuel reforming. In the hydrocarbon fuel reformers, the fuel, such as gasoline, ethanol, methane, and methanol, can be converted into hydrogen-rich gas through steam reforming (STR) or autothermal reforming (ATR), followed by water gas shift (WGS) reaction and partial oxidation (PrOx) reaction. Among these available hydrocarbon fuels, methanol is a unique fuel which it is sulfur-free and can be activated at relatively low temperature (under 300 ^{o}C). Furthermore, the steam reforming of methanol features low content of carbon monoxides. [1-3] This could be a significant advantage from system simplification and process heat recovery points of view. Therefore, it is regarded as an attractive method for hydrogen production.

On the other hand, the microchannel reactors have been introduced to minimize a complicated steam reformer. This is mainly because the microchannel reactors merit a higher surface to volume ratio, which might be several orders of magnitude higher compared to the traditional steam reformer, and hence, the heat and mass transfer inside the micro reformer can be greatly enhanced [4]. In accordance with the information of references [5-11], it is observed that the total length and the width of the micro reformers are ranged within 10 to 80 mm, and its thickness is within 1 to 10 mm. In general, the micro reactors are equipped with a finite number of flow

channels for evenly distributing the reactant gases over the flow field for reaction. An even distribution of reactant gas over the flow field is a necessary condition for higher conversion ratio. In this regard, the geometry of the manifold and the flow network should be properly optimized toward even distribution of reactant gas. Pan, et al. [12] carried out optimal design of complex manifold geometries for even flow distribution between microchannels by means of the flow network method. Tonomura, et al. [13] performed a CFD-based optimal design of manifold in plate-fin micro devices. Balaji, et al. [14] also designed a novel structure so as to produce an even velocity distribution. Recently, Arzamendi et al. [15] performed a numerical study of the steam reforming reaction and showed that the performance of the chemical reactions could be greatly improved in the micro reactors. Furthermore, the parametric study and correlation for operation condition and geometric configuration were performed at steam reformer by Jang et al. [16]. The results have shown that the methanol conversion ratio can be improved from 32.4% to 67% for the particular case at 1 cc/min flow rate on structure of one inlet two/outlets.

The foregoing literature review indicates that no numerical models on the optimization for three-dimensional full model including multi-variables up to 20 using simplified conjugate-gradient method has been proposed. This has motivated the present investigation. Numerical studies of the methanol steam reforming process in a micro reformer are definitely essential toward understanding the physical transport phenomena inside the devices. Therefore, in this study a three-dimensional full model of the micro reformer was built for predicting the effects of the geometric and the operating parameters on the chemical reaction. The parameters considered herein include wall temperature, channel geometry, inlet and outlet manifold configuration, and flow rate. The model is used to predict the distributions of flow velocities in channel as well as the methanol conversion ratio and the mass fraction of carbon monoxide. The present study is aimed at obtaining a maximum methanol conversion ratio by adjusting the channel widths (CH1~CH20) from optimization approach of simplified conjugate gradient method (SCGM).

NOMENCLATURE

a_{ij}	stoichiometric coefficients
A	pre-exponential constant
A_{SR}, A_{CO}	pre-exponential constant
B_i	chemical symbol for the i-th species
C_k	Variables for optimization
C_F	drag coefficient
C_i	concentration of the species i
C_p	specific heat ($kJkg^{-1} K^{-1}$)
D_i	multi-component diffusivity of spices i ($m^2 s^{-1}$)
D_i^T	thermal diffusion coefficient of spices i ($m^2 s^{-1}$)
D_{ij}	multi-component diffusivity of the pair i-j ($m^2 s^{-1}$)
E_a	activation energy ($J mol^{-1}$)
h_0	total enthalpy ($J kg^{-1}$)
H	channel depth (m)
J_i	species diffusion flux ($kg m^{-2} s^{-1}$)
k_{mix}	conductivity for gas mixture ($W m^{-1} K^{-1}$)
k_p	catalyst layer permeability (m^2)
k_{ij}	thermal diffusivity ratio
k_{SR}, k_{CO}	chemical reaction coefficients
k_{fi}, k_{ri}	forward and reverse rate constants of the j-th step
l'	diffusion length scale
l	length of reformer
L	channel length (m)
m	exponent on pressure dependency
M	molecular weight ($kg kmol^{-1}$)
n	temperature exponent
p	operating pressure (Pa)
$\boldsymbol{p}$	objective function
q	heat flux ($W m^{-2}$)
$\dot{Q}$	volumetric flow rate of entering liquid mixture ($cc\ min^{-1}$)
R	universal gas constant ($J mol^{-1} K^{-1}$)
R_j	reaction rate ($kmol m^{-2} s^{-1}$)
R_e	Reynolds number ($\rho V L \mu^{-1}$)
S_c	production rates of species i in gas phase ($kmol s^{-1}$)
S_i	sources term of the pressure drop within porous media
t	thickness of reformer
T_{in}	inlet temperature (K)
T_w	top wall temperature (K)
v	velocity vector ($m s^{-1}$)
V	volume (m^3)
w	width of reformer
w_{in}	inlet manifold width (m)
w_{out}	outlet manifold width (m)
W	channel width (m)
x	mole fraction
Y_i	mass fractions of the species i

Greek symbols

α	concentration exponent
β	step size
γ	conjugate gradient coefficients
δ	catalyst layer thickness (m)
ε	catalyst layer porosity
Θ_{ij}	Chapman-Enskog parameter
μ	dynamic viscosity of the fluid (Pa s)
ξ	methanol conversion ratio
π	search directions
ρ	fluid density ($kg m^{-3}$)
τ	shear stress tensor ($N m^{-2}$)
Ω	collision integral

THEORETICAL ANALYSIS

In the catalytic micro reactor shown in Figure 1, the reactants, liquid methanol (CH_3OH) and water (H_2O), entering the micro reactor at the inlet, and due to heating process the liquid mixture is converted to the gas mixture immediately. After the steam reforming reaction in the reformer, a mixture of product gases (CO, CO_2, and H_2) along with the unconsumed reactants exits at the outlet. The microchannel reactor and its channels ribs are made of stainless steel. The channels are 500 μm wide, 600μm deep, and 33 mm long, which are machined in parallel on a flat plate in the micro reactor. The flat plate contains 20 parallel channels of rectangular cross section. In practices, a catalyst layer of 20 to 40 μm thickness is usually coated on the surface of metal for chemical reaction. In this simulation model, a 30-μm thick porous catalyst layer is chosen because it leads to higher performance according to the observation of Kim and Kwon [17].

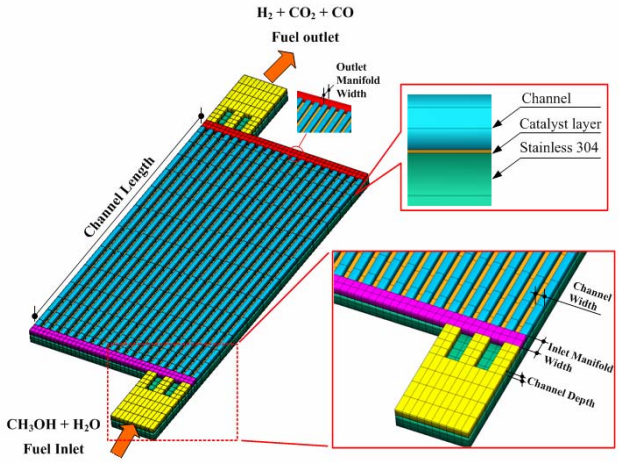

Figure 1 The structure of microchannel reformer.

The theoretical model is developed based on the following assumptions:

(1) All the species, including methanol (CH_3OH), water (H_2O), carbon monoxide (CO), carbon dioxide (CO_2), and hydrogen (H_2), are in gas phase. It is assumed that the liquid methanol is completely vaporized to gas phase immediately before entering the inlet.
(2) The gas flow in the reformer is assumed to be incompressible, steady, and laminar.
(3) The influence of gravity on the flow motion is negligible.
(4) The porous catalyst layer is homogeneous and isotropic.
(5) The chemical reaction takes place only in the catalyst layer.

In order to shorten the computational time, the model of governing equations was separated. The continuity and momentum equations are used at first, and then the species and energy equations are applied after the optimal channel width is found. For the continuity and momentum equations are as follows:

Continuity equation:

$$\nabla \cdot (\varepsilon \rho v) = 0 \tag{1}$$

where ε is the porosity of the catalyst layer, and ρ and v is the fluid density and velocity vector, respectively. For the pure fluid region, ε=1.

Momentum equations:

$$\nabla \cdot (\varepsilon \rho v v) = -\varepsilon \nabla p + \nabla \cdot (\varepsilon \mu_{mix} \nabla v) + S_i \tag{2}$$

where p is the pressure, μ_{mix} is the dynamic viscosity of the fluid. The local dynamic viscosity is established based on the Chapman-Enskog theory for multi-component gas mixtures at low density introduced by Bird, Stewart and Lightfoot [18]. where M_i represents the molecular weight of species i. In addition, in equation (2) the source term S_i only exists for the flow in the porous catalyst layer and is expressed as [19]

$$S_i = -\frac{\varepsilon^2 \mu v}{k_p} - \frac{\varepsilon^3 C_F \rho}{\sqrt{k_p}} |v| v \tag{3}$$

where k_p is the permeability and C_F is the drag coefficient. Here in the catalyst layer, $k_p = 2.379\times10^{-12}$ m^2 and $C_F = 0.55$. Note that in the pure fluid region, $k_p = \infty$ and $S_i = 0$.

Optimizer – SCGM Method

The SCGM method presented by Cheng and Chang [23] is employed as the optimization scheme. This study is aimed at optimization of the widths for the channels so that an even distribution of the velocity in the channels can be obtained. Therefore, the objective function in conjunction with the optimization process is defined in the following:

$$\boldsymbol{P} = \left\{ \left[\sum_{n=1}^{20} \left(v_{CHn} - v_{avg} \right)^2 \right] \frac{1}{20} \right\}^{0.5} / v_{avg} \tag{4}$$

where v_{CHn} denotes the average velocity in channel n, which is determined by integrating the cross-sectional velocity distribution with respect to local area for each channel, and v_{avg} represents the average velocity can be calculated by

$$v_{avg} = \left(\sum_{n=1}^{20} v_{CHn} \right) / 20 \tag{5}$$

The optimization of the flow channels is for evenly distributing the velocity of the reactant gases over the flow field for reaction. On the other hand, the widths of the 20 channels are regarded as the parameters to design, which are denoted by C_n with n=1, 2,…,20. Note that the objective function is defined in

terms of the standard deviation of velocity in the 20 channels. In this manner, the uniformity of the velocity in the channels is expected to be greatly improved as the magnitude of the objective function (***P***) is minimized. The simplified conjugate gradient method evaluates the gradients of the objective function and sets up a new conjugate direction for the updated solutions with the help of a sensitivity analysis. The initial guess for each designed parameter is made first, and in the successive steps the conjugate gradient coefficients and the searching directions are evaluated. The new design variables are continuously updated. When the objective function reaches a minimum, the optimization process is completed and the searching procedure is then terminated. In general, in a finite number of iterations the convergence can be achieved. Since general descriptions and further details of the method are available in (Cheng and Chang [23]), the procedure of the optimization process for the present problem is described briefly in the following.

1. Make an initial guess for the widths of the 20 channels $\{C_k, k=1, 2,\ldots,20\}$.
2. Use the direct problem solver to predict the three-dimensional momentum transport phenomenon and calculate the value of the objective function (***P***) by equation (4). When the objective function reaches a minimum, the solution process is terminated. Otherwise, proceed to step (4).
3. Perform the direct numerical sensitivity analysis to determine the gradient functions $(\partial \boldsymbol{P}/\partial C_k)^n$ (k=1, 2,…, 20). First, give a perturbation (ΔC_k) to each of the designed parameters $\{C_k, k=1, 2,\ldots,20\}$, and then find the change in the objective function ($\Delta \boldsymbol{P}$) caused by ΔC_k. Then, the gradient function with respect to each of the designed parameters $\{C_k, k=1, 2,\ldots,20\}$ can be calculated by the direct numerical differentiation as

$$\frac{\partial \boldsymbol{P}}{\partial C_k} = \frac{\Delta \boldsymbol{P}}{\Delta C_k} \tag{6}$$

4. Calculate the conjugate gradient coefficients γ_k^n and the search directions π_k^{n+1} for each of the designed parameters $\{C_k, k=1, 2,\ldots,20\}$ with

$$\gamma_k^n = \left[\frac{(\frac{\partial \boldsymbol{P}}{\partial C_k})^n}{(\frac{\partial \boldsymbol{P}}{\partial C_k})^{n-1}} \right]^2 \tag{7}$$

k=1, 2,…,20

$$\pi_k^{n+1} = (\frac{\partial \boldsymbol{P}}{\partial C_k})^n + \gamma_k^n \pi_k^n \tag{8}$$

k=1, 2,…,20

The value of conjugate gradient coefficients at n=0 is typically set to be zero as a start.

5. Assign values to the step sizes β_k (k=1, 2,…,20) for all the designed parameters $\{C_k, k=1, 2,\ldots,20\}$. Typically, those values are chosen within 0.01 to 0.001 after a trial-and-error process.
6. Update the widths of the 20 channels (C_k, k=1, 2,…,20) with

$$C_k^{n+1} = C_k^n - \beta_k \cdot \pi_k^{n+1} \qquad k=1, 2,\ldots,20 \tag{9}$$

and then go back to step (2).

Detailed information for determining the magnitudes of the perturbations (ΔC_k) and the step sizes (β_k) was described by Cheng and Chang [23]. Here in this study, the typical value for ΔC_k is assigned to be 0.05 mm, and the value of β_k is switched from 0.01, 0.005, and then to 0.001 in accordance with the convergence level in the optimization process. A smaller value of β_k is specified as the iterative design approaches the optimal solution. The flow chart of the optimization process is plotted in Figure 2a. The self-developed optimizer, the commercial CFD code, and the pre-processor are connected through an interface program. The interface program is written by Python language. Using the interface it is possible to pass messages among the direct problem solver, the optimizer, and the pre-processor to update the geometrical model and generate grid system for computation. The message of necessary changes in the designed parameters suggested by the optimizer is sent to the pre-processor for building the updated geometrical model and generating grid system for computation. Next, the direct problem solver is executed based on the updated information to yield the numerical predictions of the flow fields and the objective function as well, which are further transferred back to the optimizer for calculating the consecutive searching directions. Connection among the optimizer, the direct problem solver, and the pre-processor is shown in Figure 2b. Searching the 20 variables is time-consuming but unavoidable. Therefore, the distributed computations are designed to run the 20 cases at the same time in order to increase the efficiency of computation. The five personal computers with quad core are connected by switch hub. Through the free software PSEXEC, Fortan program, and five computers, the optimizer can perform the maximum cases of 24 cases in the meantime in operation system with windows server 2003 (Figure 2c).

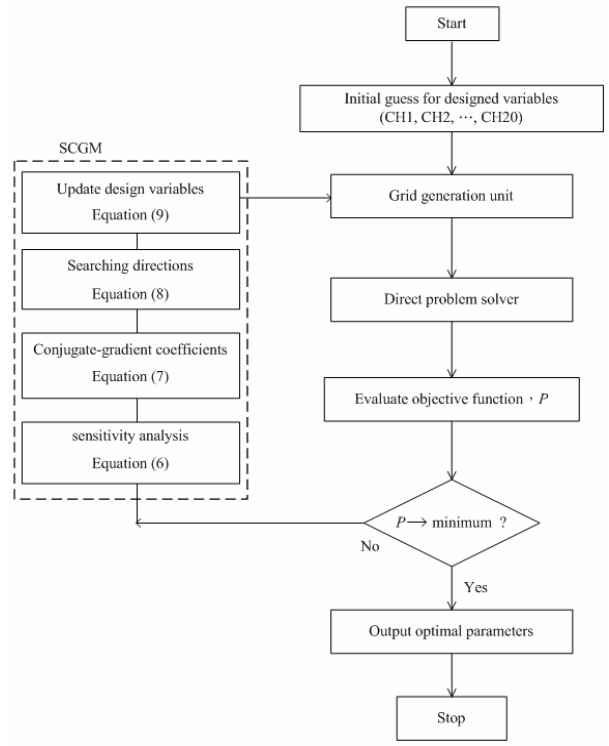

(a) Flow chart of optimization process.

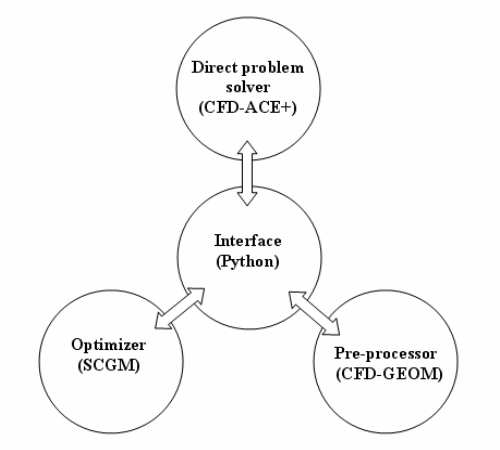

(b) Connection among optimizer, direct problem solver, and pre-processor

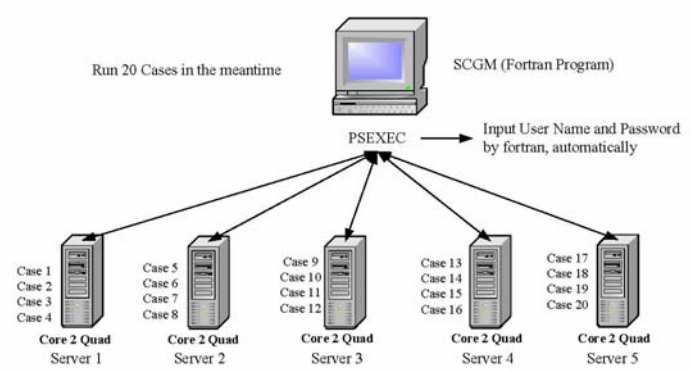

(c) Structure of distributed computing.

Figure 2 Optimization process and Structure of distributed computing.

At the second part, when the optimum channel width distributions are obtained by SCGM with minimum objective function, the energy and species equations are combined with equations of first part to solve and evaluate the performance of steam reformer. The energy and species equations are as follow.

Energy equation:

The steady-state energy conservation equation is given as

$$\nabla \cdot \left(\varepsilon \rho v h_0 \right) = \nabla \cdot q + \varepsilon \tau : \nabla v + \varepsilon \frac{dp}{dt} \tag{10}$$

where h_0 is the total enthalpy; τ is the shear stress tensor. The heat flux term q accounts for thermal conduction and energy transport by species diffusion determined as follows:

$$q = -k_{mix} \nabla T + \sum_{i=1}^{N_G} h_i J_i \tag{11}$$

where N_G is total number of gas-phase species and h_i is the specific enthalpy of species i. As suggested by Bird, et al. [18], thermal conductivity k_{mix} of a gaseous mixture is calculated using the mixture kinetic theory and is written as

$$k_{mix} = \sum_{i=1}^{N_G} \frac{x_i k_i}{\sum_{j=1}^{N} x_j \Theta_{ij}} \tag{12}$$

Spices equation:

$$\nabla \cdot \left(\varepsilon \rho v Y_i \right) = \nabla \cdot J_i + S_C \tag{13}$$

where Y_i is the mass fraction of species i, and S_c is the production rates of i-th spices in gas phase. The species diffusion flux may be written as suggested in Ref.[18]:

$$J_i = \rho D_i \nabla Y_i + \rho D_i^T \frac{\nabla T}{T} + \frac{\rho Y_i}{M} D_i \nabla M - \rho M \sum_j D_j \nabla Y_j - \rho \nabla M \sum_j D_j Y_j - \rho Y_j \sum_j D_i^T \frac{\nabla T}{T} \quad (14)$$

Chemical rate expressions:

The reactants flowing through the pores in a porous solid arrive at the solid catalyst surface by diffusion. At the catalyst surface, in the absence of any deposition or etching, the diffusion flux is exactly balanced by the reaction flux, yielding a balance equation, which may be written as:

$$M_i \sum_{j=1}^{N_{steps}} (a_{ij}'' - a_{ij}') R_j = \rho D_i \nabla Y_i \quad (15)$$

where a_{ij} are integer stoichiometric coefficients, R_j is the mole reaction rate of the *j*-th reaction. In the discrete form, the balance equation for the gas-phase species may be expressed as [20]:

$$M_i \sum_{j=1}^{N_{steps}} (a_{ij}'' - a_{ij}') R_j = \rho D_i \frac{Y_i - Y_{P,i}}{l'} \quad (16)$$

where $Y_{P,i}$ denotes the species mass-fraction in the pore fluid, Y_i is the mass-fraction at the pore-fluid/catalyst interface, and the diffusion length scale is denoted by *l'*. The volumetric production rate S_c of species *i*, can be obtained from the surface flux using

$$S_c = \rho D_i \frac{Y_i - Y_{P,i}}{l'} \left(\frac{S}{V}\right)_{eff} V \quad (17)$$

where $(S/V)_{eff}$ is the effective surface area on which the catalytic reactions occur per unit volume of the catalyst layer, and *V* is the volume of the control volume under consideration. In addition, the reaction rates R_j of the *j*-th reaction appearing in equation (16) is determined based on the mechanism of the multi-step reaction occurring at the surface of the catalyst clusters. For example, in the reformer the reactions are

$$\text{Reaction 1 : } CH_3OH + H_2O \rightarrow 3H_2 + CO_2 \quad (18)$$
$$\text{Reaction 2 : } CO_2 + H_2 \rightarrow CO + H_2O \quad (19)$$

Therefore, R_1 and R_2 can be determined, as suggested in Ref. [21], with

$$R_1 = k_{f1} C_{CH_3OH}^{\alpha_{1a}} C_{H_2O}^{\alpha_{1b}} \quad (20)$$
$$R_2 = k_{f2} C_{CO_2}^{\alpha_{2a}} C_{H_2}^{\alpha_{2b}} \quad (21)$$

where α_{1a}, α_{1b}, α_{2a} and α_{2b} are concentration exponents, and the chemical reaction rate coefficients, k_{f1} and k_{f2}, can be expressed as follows:

$$k_{f1} = A_1 T^n (p / p_{atm})^m \exp(-E_{a1} / RT) \quad (22)$$
$$k_{f2} = A_2 T^n (p / p_{atm})^m \exp(-E_{a2} / RT) \quad (23)$$

where *A*, n, *m*, E_a, and *R* represent the pre-exponential constant, temperature exponent, exponent on pressure dependency, activation energy, and gas constant, respectively. The information of these coefficients corresponding to Reactions 1 and 2 are provided by Pan and Wang [22].

Boundary conditions

In this study, the volumetric flow rate of the entering liquid mixture ($\dot{Q}$) is varied from 0.1 ~ 0.6 cc min^{-1}. The liquid is assumed to be vaporized and become the gas mixture before entering the inlet. The steam to carbon ratio is fixed at 1.1. The temperature of the entering gas mixture at the inlet is maintained at 393 K. In this manner, the mass fraction of methanol (Y_{CH3OH}) is fixed at 0.618 and that of water (Y_{H2O}) is 0.382. The outer surface of the reformer is assumed to be ideally insulated except the top surface. In practices, the top surface is heated by an electrical heater or a combustor to maintain at a high temperature in order to supply thermal energy to the reformer for the steam reforming reaction. In this study, the temperature of the hot bottom wall of the stainless steel (T_w) is assumed to be uniform over the wall. The temperature is maintained at a value of 533 K for extensively investigating the effects of the heating temperature on the performance of the micro reformer. The back pressure is assigned to be 101,325 Pa.

Numerical methods

The commercial package, CFD-ACE+, is used to build the three-dimensional simulation model for the solutions of transport phenomena inside the micro reformer. The package is developed based on SIMPLEC algorithm and finite-volume method. A structured multi-grid solver is chosen in computation with a convergence criterion of 1×10^{-6} for all quantities. A grid system of 210,000 grid points is adopted typically in the computation domain. Computations were performed on a personal computer with Intel Core™ 2 Quad 2.6G CPU. Typical computation time for a single case required more than 120 minutes. In the present work, channel width configurations were taken into consideration, which is plotted in Figure 1. The cross section areas of the inlet and the outlet are equal and fixed at 5 mm × 0.6 mm.

RESULTS AND DISCUSSION

Figure 3 shows the variation in the objective function during the optimization process for the six cases. It is observed that the value of the objective function is continuously decreased in the optimization process for all cases. The numbers of iterations required to reach the optimal designs are roughly 21, 27, 35, 36, 47 and 56 for inlet flow rate from 0.1 to 0.6 cc min^{-1}. The iteration numbers of boundary condition for inlet flow rate 0.6 cc min^{-1} is lager than other cases. It is also found that the magnitude of the objective function in case 6 has the highest value. This might be that the 0.6 cc min^{-1} flow rate cause high uneven velocity distribution comparing to others.

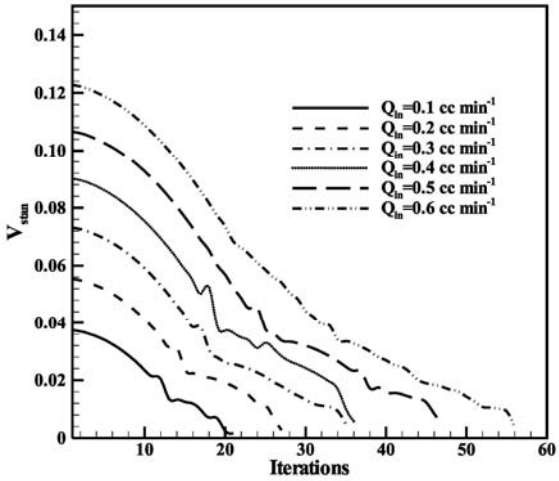

Figure 3 Convergence process of the objective function.

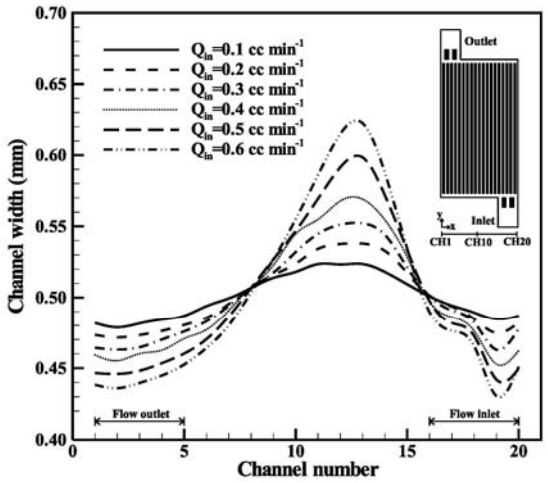

Figure 4 Channel width distributions for various cases of inlet flow rates from 0.1 to 0.6 cc min^{-1}.

The channel widths distribution for uniform velocity was obtained from optimization searching work, as shown in Figure 4. When the inlet flow rate is increased, the channel widths of number 11 to 14 are also increased. It is probably because channels number 11 to 14 are the dead zones (low-velocity zone) due to the parallel channel arrangement. Therefore, the channel widths for channel number 11 to 14 were adjusted to magnify by simplified conjugate gradient method. On the other hand, the channel number 1-5 and 16-20 is decreased as the inlet flow rate is increased. Note that the channel widths distribution from channel number 16 to 20 displays a wavelike. It is due to the inlet of the flow is design on the right hand side of the model.

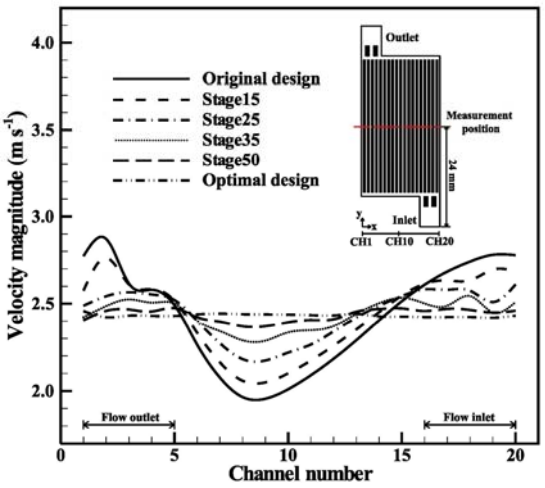

Figure 5 Velocity distributions for inlet flow rates 0.6 cc min^{-1}.

In order to discuss and show the low-velocity zone in the simulation model, the velocity distribution in channels for various stages in optimization process is plotted in Figure 5 and the average velocity is acquired from xz cut for each channel at y=24 mm. According to the velocity distribution for original design, the middle of the simulation model presented a low-velocity zone (CH6~CH13), and the high velocity zone shows on the double side (CH1~CH5 and CH15~CH20). The channel widths are adjusted toward the low velocity standard deviation by optimization searching the uniform velocity is obtained on Stage 53.

In prior to the parametric study of the effects of the geometric and the operating conditions, the simulation model is validated by a comparison with some existing experimental data. Figures 6(a) and 6(b) show the comparisons between the present predictions and the experimental data provided by Seo, et al. [24] in the methanol conversion ratio and the compositions of product gases in the dry reformate, respectively. The conditions of the case shown in this figure are the same as conditions described in [24]. In this case, the reformer is with 20 channels of L=3.3×10^{-2} m, W=5.0×10^{-4} m, and H=6.0×10^{-4}; the thickness of the catalyst layer is 3.0×10^{-5} m; the inlet temperature is set to be 393 K; and the volumetric flow rate is varied within 0.1 and 1.0 cc min^{-1}. Other parameters are identical to those given with the values displayed in Table 1 of ANNEX. In this figure, it is clearly that the methanol conversion ratio is reduced by increasing the volumetric flow rate or decreasing the wall temperature. For

the case at T_w=533 K and $\dot{Q}$=0.1 cc min^{-1}, the methanol conversion ratio may achieve 97%; however, it is less than 20% at T_w=473 K and $\dot{Q}$=0.6 cc min^{-1}. As to the compositions of product gases in the dry reformate, it appears that at $\dot{Q}$=0.1 cc min^{-1}, the mole fractions of H_2 and CO_2 are approximately at 73~75% and 23~25%, respectively. On the other hand, it is found that when the wall temperature is increased from 473 K to 533 K, the mole fraction of CO is elevated from 0.1% to 1.6%. The experimental data provided by Seo, et al. [24] closely agree with the present numerical predictions, especially for the compositions of product gases in the dry reformate.

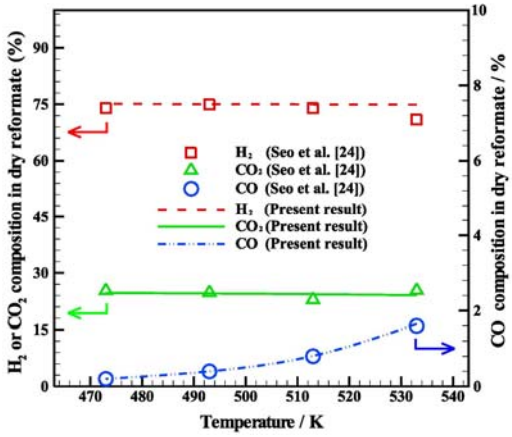

(a) Methanol conversion ratio

(b)

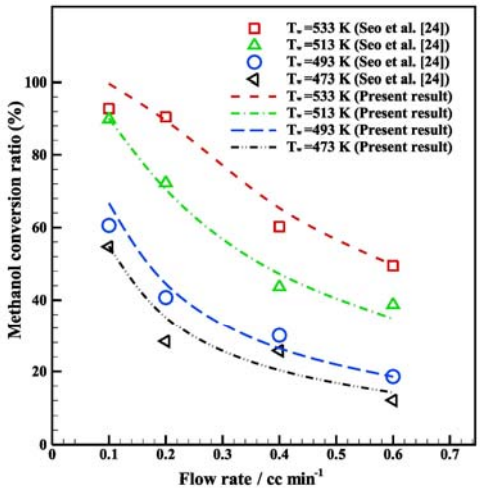

(c) Gas composition (mole fraction) at $\dot{Q}$=0.1 cc min^{-1}.

Figure 6 Comparison between present predictions and experiments [24].

Figure 7 shows the comparison in reforming performance between the optimal and the original designs at T_w=533 K. It is found that the conversion ratio is significantly improved from 54.17 % to 62.62 % at $\dot{Q}$=0.6 cc min^{-1}. However, the mole fraction of carbon monoxide is increased from 2.85 % (original) to 5.21 % (optimal) at $\dot{Q}$=0.6 cc min^{-1}. At a higher flow rate $\dot{Q}$=0.6 cc min^{-1}, both designs leads to a high mole fraction of carbon monoxide distributions. This is probably because the high concentration of H_2 causes the reverse water gas shift reaction to increase the production rate of CO, as predicted in equation (12).

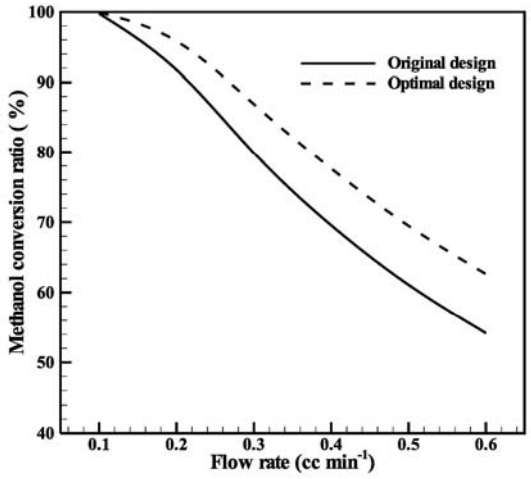

(a) Methanol conversion ratio

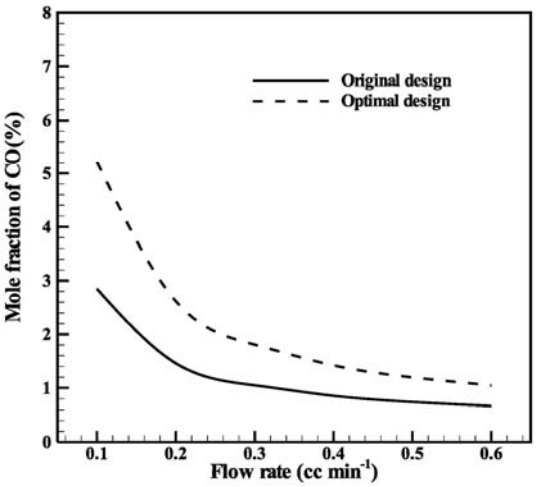

(b) Mole fraction of CO

Figure 7 Comparison in methanol conversion ratio and mole fraction of carbon monoxide between the original and the optimal designs.

CONCLUTION

In this study a three-dimensional simulation model of the micro reformers is built for increasing the methanol conversion

ratio. It is found that the numerical predictions by the simulation model closely agree with the experimental data provided by Seo, et al. [24].

An optimum searching study of the dependence of methanol conversion ratio on the channel widths and the operating conditions has been performed. According to the numerical results of the optimal algorithm, an optimal distribution of the channel widths is suggested and compared with the original base-line set. Comparison in reforming performance between the optimal and the original designs shows that the conversion ratio is significantly improved from 54.17 % to 62.62 % at $\dot{Q}$ =0.6 ccmin^{-1}. Therefore, the channel widths distribution optimization for uniform velocity can indeed increase the efficiency of steam reformer.

ACKNOWLEDGMENTS

Financial support for this work was provided by the National Science Council, Taiwan, under grant NSC 97-2221-E-006 -110 -MY2.

REFERENCES

[1] D.R. Palo, R.A. Dagle, J.D. Holladay, "Methanol steam reforming for hydrogen production," Chem. Rev., Vol. 107, pp. 3992-4021, 2007.

[2] F. Joensen, J.R. Rostrup-Nielsen, "Conversion of hydrocarbons and alcohols for fuel cells," J. Power Sources, Vol. 105, pp. 195-201, 2002.

[3] L.F. Brown, "A comparative study of fuels for on-board hydrogen production for fuel-cell-powered automobiles," Int. J. Hydrogen Energy, Vol. 26, 381-397, 2001.

[4] W. Ehrfeld, V. Hessel, H. Lowe, "Microreactors: New technology for modern chemistry," Wiley-VCH, Weinheim, 2000.

[5] K.F. Jensen, "Microreaction engineering-is small better?," Chemical Engineering Science, Vol. 56, pp. 293-303, 2001.

[6] W. Stefanie, F. Günter, B. Reinhard, B. Manfred, L. Marcel, "Fluiddynamische aspekte in mikrostrukturreaktoren," Chemie Ingenieur Technik, Vol. 71, pp. 447-455, 1999.

[7] S. Tanaka, K. S. Chang, K. B. Min, D. Satoh, K. Yoshida, M. Esashi, "MEMS-based components of a miniature fuel cell/fuel reformer system," Chemical Engineering Journal, Vol. 101, pp. 143-149, 2004.

[8] Y. Kawamura, N. Ogura, T. Yamamoto, A. Igarashi, "A miniaturized methanol reformer with Si-based microreactor for a small PEMFC," Chemical Engineering Science, Vol. 61, pp. 1092-1101, 2006.

[9] T. Terazaki, N. Masatoshi, T. Keishi, N. Osamu, Y, Tadao, "Development of multi-layered microreactor with methanol reformer for small PEMFC," Journal of Power Sources, Vol. 145, pp. 691-696, 2005.

[10] J.D. Holladay, J.D. Holladay, E.O. Jones, R.A. Dagle, G.G. Xia, C. Cao, Y. Wang, "High efficiency and low carbon monoxide micro-scale methanol processors," Journal Power Sources, Vol. 131, pp. 69-72, 2004.

[11] G. Chen, Q. Yuan, H. Li, S. Li, "CO selective oxidation in microchannel reactor for PEM fuel cell," Chemical Engineering Journal, Vol. 101, pp. 101-106, 2004.

[12] M. Pan, Y. Tang, L. Pan, L. Lu, "Optimal design of complex manifold geometries for uniform flow distribution between microchannels," Chemical Engineering Journal, Vol. 137, pp. 339-346, 2008.

[13] O. Tonomura, S. Tanaka, M. Noda, M. Kano, S. Hasebe, I. Hashimoto, "CFD-based optimal design of manifold in plate-fin microdevices," Chemical Engineering Journal, Vol. 101, pp. 397-402, 2004.

[14] S. Balaji and S. Lakshminarayanan, "Improved design of microchannel plate geometry for uniform flow distribution," The Canadian Journal of Chemical Engineering, Vol. 84, pp. 715-721, 2006.

[15] G. Arzamendi, P. M. Diéguez, M. Montes, M.A. Centeno, J.A. Odriozola, L.M. Gandía, "Integration of methanol steam reforming and combustion in a microchannel reactor for H_2 production: A CFD simulation study," Catalysis Today, Vol. 143, pp. 25-31, 2009.

[16] J. Y. Jang, Y. X. Huang, C. H. Cheng, "Investigation of effects of geometric and operating conditions on hydrogen production performance of a micro methanol steam reformer," submitted to Chemical Engineering Science.

[17] T. Kim, S. Kwon, **"**Design, fabrication and testing of a catalytic microreactor for hydrogen production**,"** Journal of micromechanics and microengineering, Vol. 16, pp. 1760-1768, 2006.

[18] R.B. Bird, W. E. Stewart, E. N. Lightfoot, "Transport phenomena," Wiley, New York, 1960.

[19] D. A. Nield and A. Bejan, "Convection in porous media," 2nd ed., p.9, Springer, New York, 1999.

[20] Dagan, G., "Flow and Transport in Porous Formations." Springer-Verlag, Berlin, 1989.

[21] Coltrin, M. E., Kee, R. J., and Rupley, F. M., "Serface chemkin: A gerenal formalism and software for analyzing heterogeneous chemical kinetics at a gas-surface interface," International J. Chem. Kinetics, Vol. 23, pp. 1111-1128, 1991.

[22] Pan, L., Wang, S., "Modeling of a Compact Plate-Fin Reformer for Methanol Steam Reforming in Fuel Cell Systems," Chemical Engineering Journal, Vol. 108, pp. 51-58, 2005.

[23] Cheng, C. H.; Chang, M. H., "A Simplified Conjugate-gradient Method for share Identification Based on Thermal Data," Numer. Heat Transfer, Vol. 43, pp. 489-

507, 2003.
[24] D. J. Seo, W. L. Yoon, Y. G. Yoon, S. H. Park, G. G. Park, C. S. Kim, "Development of a micro fuel processor for PEMFCs," Electrochimica Acta, Vol. 50, pp. 719-723, 2004.
[25] A.V. Pattekar, M.V. Kothare, "A microreactor for hydrogen production in micro fuel cell applications," Journal of Microelectromechanical Systems, Vol. 13, pp. 7-18, 2004.

W (m)	$3.0\times10^{-4}\sim 9.0\times10^{-4}$
H (m)	6.0×10^{-4}
w_{in} (m)	1.0×10^{-3}
w_{out} (m)	1.0×10^{-3}
$\dot{Q}$ (cc min^{-1})	0.1 ~ 0.6 cc min^{-1} (liquid)
T_w (K)	533
T_{in} (K)	393
R (J mol^{-1} K^{-1})	8.314
p (Pa)	101,325
ε	1
k_p (m^2)	∞
ε [25]	0.38
C_F [19]	0.55
k_p (m^2) [25]	2.379×10^{-12}
δ(m) [17]	3.0×10^{-5}
M_{H2O} (kg kg-mole^{-1})	18.015
M_{CO} (kg mole^{-1})	28.010
M_{CH3OH} (kg mole-1)	32.04
M_{CO2} (kg mole^{-1})	44.011
M_{H2} (kg mole^{-1})	2.016
σ_{H2O} (Å)	2.641
σ_{CO} (Å)	3.69
σ_{CH3OH} (Å)	3.626
σ_{CO2} (Å)	3.941
σ_{H2} (Å)	2.827
$\alpha_{SR,a}$	0.44
$\alpha_{SR,b}$	0.4
$\alpha_{CO,a}$	1.0
$\alpha_{CO,b}$	1.0
A_{SR}	9.055×10^{8}
A_{CO}	500724
$E_{a,SR}$ (kJ) [22]	108
$E_{a,CO}$ (kJ) [22]	76
n	0.8 (STR); 0.68(WGS)
m	0.

ANNEX :

Table 1 Geometric and physical conditions and fixed properties in computation

Parameter	Value
L (m)	3.3×10^{-2}